Article

Native Cryo-Correlative Light and Synchrotron X-ray Fluorescence Imaging of Proteins and Essential Metals in Subcellular Neuronal Compartments

Richard Ortega, Mónica Fernández-Monreal, Noémie Pied, Stéphane Roudeau, Peter Cloetens, and Asuncion Carmona*

Cite This: *Chem. Biomed. Imaging* 2024, 2, 744−754

Read Online

ACCESS | Metrics & More | Article Recommendations | SI Supporting Information

ABSTRACT: Essential metals such as iron, copper, and zinc are required for a wide variety of biological processes. For example, they act as cofactors in many proteins, conferring enzymatic activity or structural stability. Interactions between metals and proteins are often difficult to characterize due to the low concentration of metals in biological tissues and the sometimes labile nature of the chemical bonds involved. To better understand the cellular functions of essential metals, we correlate protein localization, using fluorescence light microscopy (FLM), and metal distribution with synchrotron X-ray fluorescence (SXRF), a high-sensitivity and high-spatial-resolution technique for metal imaging. Both chemical imaging modalities are implemented under cryogenic conditions to preserve native cell structure and chemical element distribution. As a proof of concept, we applied cryo-FLM and cryo-SXRF correlative imaging to cultured primary hippocampal neurons. Neurons were labeled under live conditions with fluorescent F-actin and tubulin dyes, then samples were flash-frozen and observed in a frozen hydrated state. This methodology, cryo-FLM combined to cryo-SXRF, revealed the distribution of iron, copper and zinc relative to F-actin and tubulin in the growth cones, dendrites, axons, and axonal *en passant boutons* of developing neurons.

KEYWORDS: *X-ray fluorescence imaging, synchrotron, metals, cryogenic, neurons, synapse, actin, tubulin*

INTRODUCTION

Inorganic chemical elements are of considerable biological importance. For instance, 10 metals—Na, K, Mg, Ca, Fe, Mn, Co, Cu, Zn and Mo—are absolutely essential for human cell function.[1,2] It is estimated that essential metals are required in the catalytic or structural sites of about one-third of the human proteome.[3,4] The balance of essential metals in the human body is a finely regulated parameter, and metal dyshomeostasis due to genetic or environmental triggers can have dramatic consequences for human health. This is particularly true in the central nervous system (CNS) with deleterious effects of metal dyshomeostasis leading to a wide range of neurological impairments, from neurodevelopmental disorders to neurodegenerative diseases.[5−7] The therapeutic restoration of metal homeostasis is a promising avenue of development for the treatment of neurodegenerative diseases.[5,8] Despite the ubiquitous involvement of essential metals in neurological processes, the study of their functions often remains challenging, mainly due to their low concentration in the brain and the labile nature of their binding with biomolecules, requiring highly sensitive analytical techniques while preserving the native chemical environment.

Imaging the native localization of metal-bound proteins in brain tissues holds great promise for deciphering the functions of metals in the CNS. For example, recent developments in native ambient mass spectrometry have enabled the imaging of a series of metal-bound proteins in brain tissue sections at a spatial resolution of 200 μm.[9] However, to obtain subcellular information, analytical techniques with higher spatial resolution need to be implemented. Multimodal correlative approaches are being developed for this purpose, often based on synchrotron X-ray fluorescence (SXRF) for metal nano-imaging.[10,11] SXRF spectrometry is a very powerful analytical tool offering high detection sensitivity, high spatial resolution on dedicated beamlines (<100 nm), and quantitative capability for metal mapping in biological samples.[12] Although SXRF cannot be performed on living cells due to cellular damage
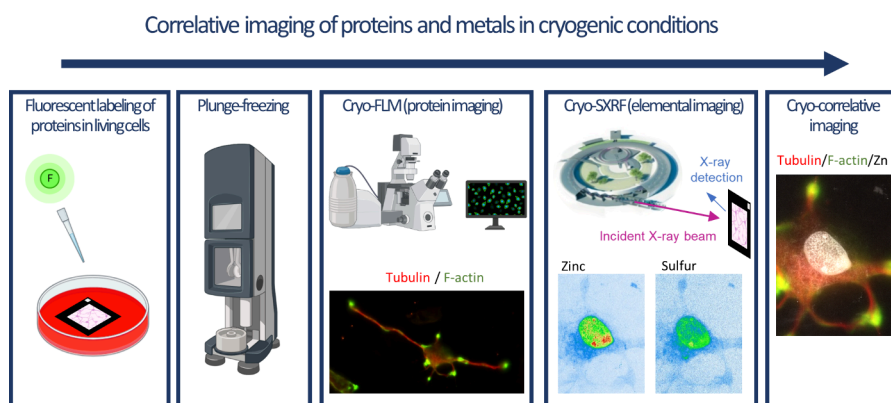
Figure 1. Methodological workflow for cryo-correlative imaging of proteins and metals in single neurons using cryo-fluorescence light microscopy (FLM) and cryo-synchrotron X-ray fluorescence (cryo-SXRF).
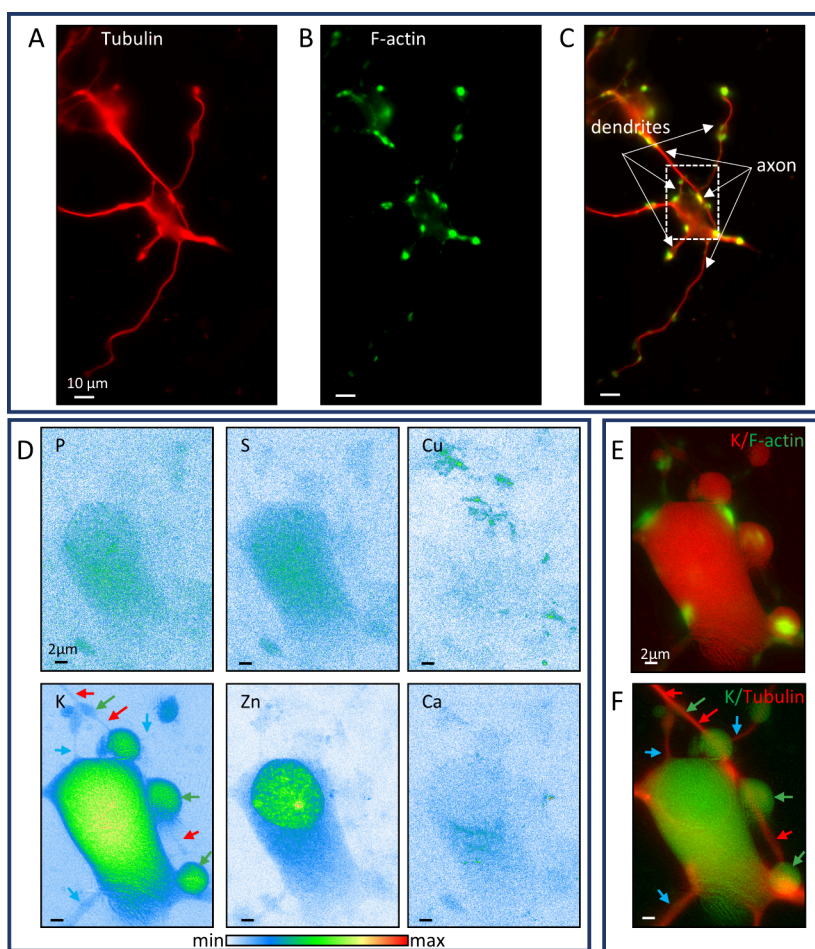

Figure 2. Cryo-correlative imaging of proteins (tubulin and F-actin) and chemical elements in developing neurons. (A) Tubulin distribution by cryo-FLM. (B) F-actin distribution by cryo-FLM. (C) Overlay image of F-actin (green) and tubulin (red), showing dendrites and axon, the dotted square represents the region of interest further analyzed by cryo-SXRF. (D) Distributions of minor elements (P, S, K, Ca) and trace metals (Cu, Zn) obtained by cryo-SXRF in the region of interest framed in C. (E, F) Examples of protein and metal overlay images generated for K and F-actin, and K and tubulin. Red arrows indicate the axon, green arrows indicate the axonal varicosities, and blue arrows indicate the dendrites.

caused by intense irradiation, SXRF can be performed under cryogenic conditions, enabling imaging of the native intracellular distribution of elements.[13−17]

SXRF imaging can be combined with other microscopy or spectro-imaging techniques to complement the information acquired on metal distribution with biological indicators such as cell compartments and organelles.[13,15,16,18−24] More

specifically, knowing the colocalization of metals with proteins at the subcellular level is an important piece of information for understanding metal−protein interactions in cells.[11,25−28] However, the protocols usually employed in cell biology for imaging proteins with fluorescently labeled antibodies are based on chemical fixation and are known to alter the quantitative content and distribution of the elements.[12,18,29−33]
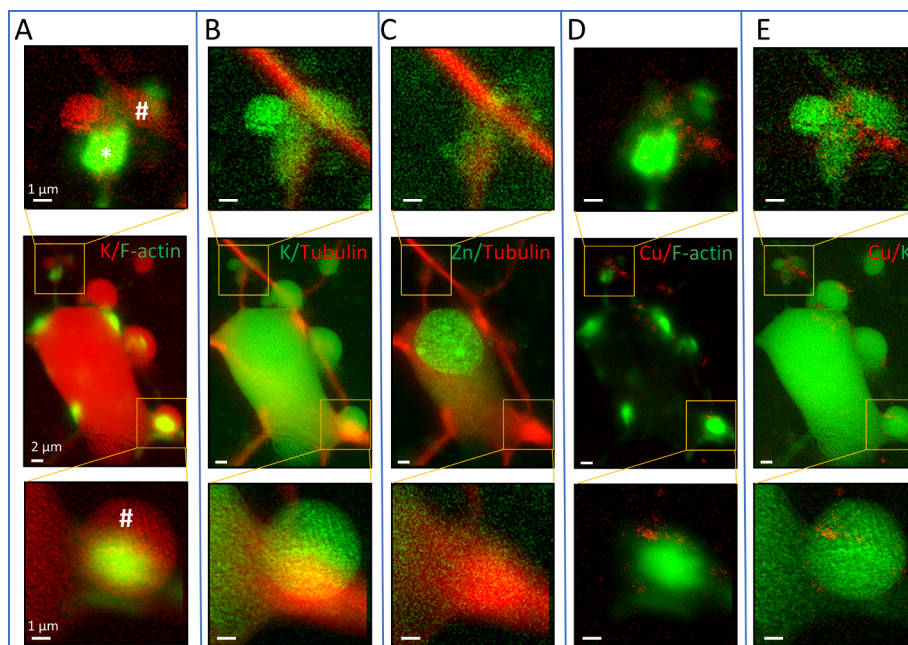
Figure 3. Cryo-correlative imaging of proteins (tubulin and F-actin) and chemical elements in a developing neuron. (A) Overlay images of K (red) and F-actin (green) (# = axonal varicosity and * = dendritic protrusion). (B) Overlay images of K (green) and tubulin (red). (C) Overlaid images of Zn (green) and tubulin (red). (D) Overlaid images of Cu (red) and F-actin (green). (E) Overlay images of Cu (red) and K (green).

To avoid this denaturing step of chemical fixation, protein labeling can be performed with fluorescent dyes developed for live-cell microcopy. We have designed correlative approaches for imaging proteins by fluorescence light microscopy (FLM) in living cells and subsequent imaging of chemical elements by SXRF.[15,25,26,28,34] Live-cell FLM can be performed using epifluorescence, confocal or super-resolution microscopy, characterized by different spatial resolutions ranging from submicron to tenth-nanometer scale. After live-cell FLM, samples are flash frozen and freeze-dried, followed by SXRF imaging. Although this strategy enables correlative imaging of proteins and metals in cells, it can still be improved. For example, the location of mobile structures, such as proteins in cytoplasmic vesicles, can change during the time elapsed between live-cell FLM observation and sample cryo-preservation, hampering the colocalization process. In addition, the freeze-drying step can lead to shrinkage of certain cellular structures.[28] Ideally, correlative imaging of metals and proteins should be performed at cryogenic temperature for FLM and SXRF. Today, SXRF imaging can be performed under cryogenic conditions on several synchrotron facilities.[13,14,17,35−37] However, the rise of cryo-CLEM (correlative light and electron microscopy)[38] has widened access to cryo-FLM using commercially available microscopes, initially intended for cryo-CLEM but which could be adapted to other cryo-FLM correlative modalities.

Hence, in this article, we present a workflow for correlating the native distribution of proteins and metals, using FLM and SXRF, respectively, both techniques implemented under cryogenic conditions on the same regions of interest. We have applied this methodological process to correlate the distribution of essential metals and cytoskeleton proteins, F-actin and tubulin, in developing hippocampal neurons.

■ RESULTS

Methodological Workflow

We have established and experimentally validated a methodological workflow for cryo-correlative imaging of proteins and metals in cultured neurons by combining cryo-FLM and cryo-SXRF (Figure 1). The workflow was applied to imaging primary rat hippocampal neurons in culture, but could be adapted to any other adherent cultured cells. First, neurons are seeded on silicon nitride membranes which are thin, flat, rigid, transparent, and chemically pure substrates enabling FLM and SXRF spectroscopic imaging. Proteins of interest are fluorescently labeled in living conditions using cell-permeable fluorescent dyes. In a second step, samples are deep-frozen, to preserve the distributions of protein and elements close to their native state. Frozen samples can be stored in liquid nitrogen until analysis. The third step is to obtain the regions of interest and their coordinates by cryo-FLM, maintaining the sample at low temperature using liquid nitrogen. The fourth step is to image the distribution of elements by cryo-SXRF in the same regions of interest. Following these steps, image correlation can be undertaken without any ambiguity.

Cryo-correlative Imaging of Cytoskeleton Proteins and Essential Metals in Developing Neurons

Primary rat hippocampal neurons at DIV3 were labeled for tubulin and F-actin fluorescence, two cytoskeleton proteins involved in neuronal development. Cryo-FLM images show a homogeneous distribution of tubulin along axonal and dendritic processes (Figures 2 A and 4A), and a spot distribution of F-actin in these neuronal processes, including distal ends and growth cones (Figure 2B and 4B), as expected for these proteins.[26,39,40] These examples validate the feasibility of cryo-FLM using SiR fluorescent dyes for F-actin and tubulin on cultured neurons, showing a high intensity fluorescent signal and low background autofluorescence.

Cryo-SXRF was performed on the regions of interest as shown in Figure 2D. In this example, the region of interest was defined to include a soma and its dendritic extensions and an axon from another neuron visible in the upper left of Figure 2A−C. This region of interest is bounded by the white dotted rectangle in Figure 2C, with a scanned area of 27.48 × 38.88 μm^2. The cryo-SXRF images show the distribution of minor (P, S, K, and Ca) and trace elements (Cu, Zn) (Figure 2D). The position of the nucleus in the soma is highlighted by the distributions of P, S, K, and Zn, including some hot spots in the nucleoli. Rounded K structures are also clearly visible along the axon, originating from the upper neuron and passing next to the analyzed neuron, revealing axonal varicosities. The relevance of the distributions of the elements will be detailed in the Discussion section. Overall, their distribution in subcellular compartments argues in favor of good preservation of cellular structures. Using the ICY software and the eC-CLEM plugin, the images coming from the two microscopy modalities have been superimposed (Figure 2E and F). The overlay images show that K colocalizes with F-actin in the axonal varicosities (Figure 2D and 2E, green arrows). Potassium correlates with tubulin along axonal and dendritic arbors (Figure 2E, red and blue arrows).

Zoom-in areas of protein/metal correlation images are shown in Figure 3. Potassium is a ubiquitous and diffusible intracellular element, meaning that it is distributed throughout the intracellular volume and can be used as an internal reference element for cell shape. Potassium is present in the cytoplasm and the nucleus, in axons and dendrites. In axonal varicosities, F-actin localization is narrower than that of K, indicating subcompartmentalization within the axonal varicosities (marked with # in Figure 3A, top and bottom panels).

F-actin is also present in patches in the peripheral region of the soma, and in a postsynaptic protrusion extending from the soma and facing the axonal varicosity (marked with * in Figure 3A, top panel). Tubulin follows the K distribution all along the axon and the dendrites (Figure 3B). Tubulin colocalizes with K in the postsynaptic protrusion (marked with an * in Figure 3A), but is not present in the axonal varicosities. Figure 3C shows the localization of Zn and tubulin. The top panel shows that both the axonal varicosity and the dendritic protrusion contain zinc. Interestingly, Cu and F-actin overlay images show that Cu is localized at the edges of F-actin rich structures (Figure 4D). Furthermore, K and Cu overlay images show that Cu is present in narrow regions around K structures, both the axonal varicosity and the dendritic protrusion (Figure 4E).

In addition to the imaging of the soma, axonal and dendritic processes shown in Figures 2 and 3, cryo-correlative imaging was applied to growth cones, which are characteristic features of developing neurons (Figure 4). Growth cones are neuronal structures that appear at the very beginning of neuro-development, at the tip of neuronal processes, responsible for development, guidance and neuronal connections.[41] Growth cones display a highly segregated distribution of F-actin and tubulin (Figure 4A−C). Cryo-FLM images show a homogeneous distribution of tubulin along the neurite, which is interrupted and extended by F-actin fluorescence in the growth cone (Figure 4A−C). Using cryo-SXRF, the distribution of physiological elements in the regions of interest framed in Figure 4C was obtained (Figure 4D). P, S, K, and Zn are present throughout the growth-cone with distinct and heterogeneous distributions, whereas Ca and Fe are localized only in the basal region, with micrometric rounded vesicle-like
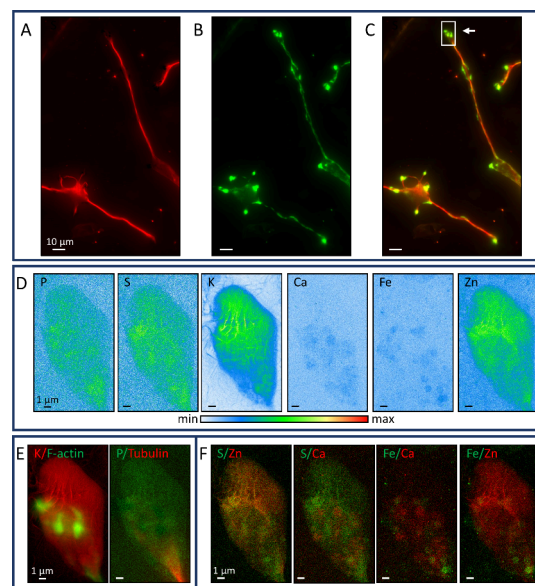

Figure 4. Cryo-correlative imaging of proteins (tubulin and F-actin) and of chemical elements in a growth cone of developing-neurons. (A) Tubulin distribution obtained by cryo-FLM. (B) F-actin distribution obtained by cryo-FLM. (C) Overlay image of F-actin (green) and tubulin (red). (D) Chemical element distributions obtained by cryo-SXRF in the growth cone area framed in C. (E) Overlay images of cytoskeleton proteins and chemical elements: potassium (red)/F-actin (green) and phosphorus (green)/tubulin (red). (F) Overlay images of minor and trace elements to highlight colocalization (S/Zn) at the inner layer border or differences in their distribution (S/Ca, Fe/Ca, and Fe/Zn).

distributions (Figure 4D). Although P, S, K, and Zn are distributed throughout the growth cone, they display distinct and heterogeneous distributions. Interestingly, the overlay of SXRF and FLM images (Figure 4E) shows that F-actin is present in discrete regions of the growth cone, in the central region (see K/F-actin overlay image), and tubulin is detected only at the base of the growth cone (see P/tubulin overlay image). Overlay images of minor and trace elements reveal some colocalization (S/Zn) and differences in distribution (Fe/Ca) (Figure 4F). The relevance of the protein and element distributions will be discussed below.

■ DISCUSSION

State-of-the-Art for Protein-Metal Correlative Imaging

The procedure described for cryo-correlative imaging of metals and proteins has been made possible by the increasing availability of cryo-FLM, now widely used for cryo-CLEM applications, and to its combination with cryo-SXRF. We will discuss the advantages of this procedure by comparing it with the protocols implemented by alternative approaches to achieve protein and metal correlation in single cells, as schematized in Figure 5.

First, cells must be grown on specific substrates suitable for SXRF imaging, in our case silicon nitride membranes. In general, FLM is performed before SXRF, because the latter is more damaging to samples than FLM, although there are some exceptions.[21] Protein labeling can be performed either with fluorescently tagged antibodies, synthetic fluorescent dyes, or genetically encoded fluorescent proteins. When antibodies are used to label intracellular proteins for immunofluorescence
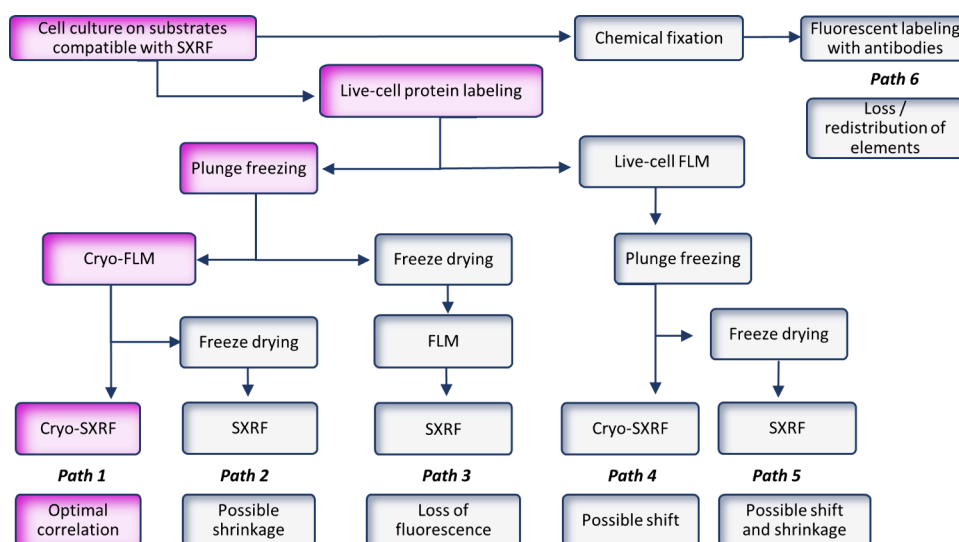
Figure 5. Schematic representation of the different methods (paths 1 to 6) developed for correlative imaging of proteins by FLM and metals by synchrotron hard X-ray fluorescence (SXRF), and potential pitfalls.

microscopy, cell membranes must be permeabilized to internalize the antibody, and the cellular structure is preserved by chemical fixation with aldehydes, embedding and dehydration with organic chemicals and solvents (Figure 5, path 6). These denaturing conditions are known to induce loss and redistribution of intracellular elements, as extensively described in the literature.[12,18,29−33] Furthermore, regardless of the elemental redistribution, chemical fixation alters the native cellular ultrastructure as compared to cryofixation.[42,43] Therefore, chemical fixation is usually not compatible with SXRF imaging of essential elements. However, in some specific cases, SXRF is applicable to chemically fixed tissues when the elements of interest (e.g., from metallic nanoparticles) are tightly bound to the biomolecules. The remaining elemental distribution, which is not lost during the chemical processing, can provide valuable information on the intracellular localization of proteins and metals or nanoparticles.[22,23] Ideally SXRF imaging of chemically fixed cells should be compared with the native distribution of the elements to get a comprehensive information on the total vs tightly bound fraction of the intracellular elements.

As an alternative to protein immunofluorescence imaging, and in order to preserve the native distribution of the essential elements, protein labeling can be performed on living cells using fluorescent dyes. In this study, we used SiR-actin and SiR-tubulin, two permeable silicon-rhodamine based fluorescent dyes with high affinity for F-actin and tubulin.[44,45] Many other commercially available fluorescent dyes can be used, for example for organelle labeling, which involves the expression of organelle-specific fluorescent proteins using a vector expressed in living cells.[46] This approach can also be extended to other genetically encoded fluorescent proteins, using transfection and expression of fluorescent protein constructs.[15,27]

After live cell protein labeling, two options can be implemented: immediate plunge-freezing (Figure 5, paths 1 to 3), or imaging proteins under live conditions by FLM prior to plunge-freezing (Figure 5, paths 4 and 5). Three main microscopy techniques can be used for live-cell protein imaging: epifluorescence, confocal or super-resolution microscopy, depending on the spatial resolution required or available. Typically, protein localization is recorded by FLM in the cell

volume, and z-stacks must be made for comparison with SXRF images, which are a 2D projection of the volumetric information.

The choice between immediate plunge-freezing (Figure 5, paths 1 to 3), or imaging proteins in living conditions by FLM before plunge-freezing (Figure 5, paths 4 and 5) is mainly motivated by the time elapsing between FLM observation and the plunge freezing step, during which dynamic intracellular components can move in living cells. If the structures of interest are highly mobile, then immediate plunge-freezing should be advocated (Figure 5, paths 1 to 3). If the structures of interest are relatively stable, not too mobile in the time frame of observation, then live-cell FLM can be performed prior to plunge-freezing (Figure 5, paths 4 and 5). In this case, samples can either be plunge-frozen and kept frozen to perform cryo-SXRF (Figure 5, path 4), or they can be plunge-frozen and freeze-dried to perform SXRF at room temperature (RT) (Figure 5, path 5). For both sequences (Figure 5, paths 4 and 5) the main drawback is a possible shift in position between the FLM and SXRF images due to the dynamics of cellular structures such as vesicles, organelles, or growth cones. If freeze-drying is used (Figure 5, path 5), then this will also cause some shrinkage of the biological structures.

Despite these limitations, both sequences have been successfully applied for correlative imaging when the structures of interest are not too mobile. For example, live-cell FLM of HeLa cells expressing a fluorescently tagged protein, huntingtin exon-1-mYFP, has been used to identify protein aggregates and compared with the location of the elemental content obtained by cryo-SXRF (Figure path 4).[27] Live-cell FLM was performed on HeLa cells expressing GFP-tagged SLC30A10 protein, a Mn-efflux transporter, and an RFP protein targeting the Golgi apparatus followed by plunge freezing, freeze-drying, and SXRF imaging at RT (Figure 5 path 5).[15] The stable position of the Golgi-apparatus within the time frame of sample preparation allowed correlative visualization of Mn accumulation in this organelle. Live-cell super-resolution microscopy (STED; stimulated emission depletion) was combined with SXRF in plunge frozen and freeze-dried cells to image post synaptic compartments and fine dendrites, distinguishing structures that cannot be resolved by confocal fluorescence

microscopy.[25,28] We have also applied this approach to the study of growth cones on developing neurons for F-actin and tubulin localization followed by plunge freezing, and freeze-drying and SXRF imaging at RT.[26,28] The correlative imaging was successful because the structural changes due to freeze-drying remained very limited, as shown by comparing FLM images of the same regions of interest before and after freeze-drying. The mobility of the growth cones was also limited by the use of SiR-tubulin and SiR-actin fluorescent dyes, which target two important cytoskeleton proteins and thus stabilize the cellular structure.

Without access to cryo-FLM, correlative imaging of mobile intracellular structures can be performed but with some severe limitations (Figure 5, path 3). Samples can be freeze-dried after plunge freezing and both FLM and SXRF can be performed at RT (Figure 5, path 3). The advantage of this approach is that the two imaging modalities are applied to the freeze-dried samples avoiding any movement of the structures and shift in position. The main disadvantage of this sequence is that the quality of FLM on freeze-dried cells is much lower than on living cells. The fluorescence of the labeling dyes is greatly reduced and depends on the nature of the fluorophore. For example protein-based fluorophores such as GFP will show a drastic or complete decrease in fluorescence intensity, probably due to the change in structure of the fluorescent protein after drying. Synthetic fluorescent dyes such as Hoechst nuclear dyes, or SiR, will retain some fluorescence but will not allow high-resolution protein imaging because the fluorescence intensity decays after drying.[18,26]

Consequently, the best results for correlative imaging are obtained by imaging protein distribution using cryo-FLM. Cryogenic conditions allow a strong fluorescence signal to be maintained, while preventing the movement of cellular structures. Ideally, cryo-SXRF should be applied after cryo-FLM, as developed in this article (Figure 5 path 1). However, if cryo-SXRF is not available on the synchrotron beamline, then samples can be freeze-dried and imaged by SXRF at RT (Figure 5, path 2). In this case, there may be some shrinkage of the cellular structures, but the correlation can still be achieved when the freeze-drying is carried out slowly with minimal cell damage. Finally, the last path is the one that offers the optimal correlative approach, labeling in living conditions, plunge-freezing the samples, with the following sequence: live-cell protein labeling, plunge freezing, cryo-FLM and cryo-SXRF, keeping the samples frozen in liquid nitrogen throughout the procedure (Figure 5, path 1). Following this path cryo-FLM and cryo-SXRF correlation can be performed without any ambiguity. A similar approach has been successfully applied in a recent study of functionalized selenium nanoparticles in cultured cancer cells showing the partial colocalization of selenium and fluorescently labeled lysosomes.[46]

Metal-Protein Correlative Cryo-Imaging in Developing Neurons

The reported cryo-FLM images of F-actin and tubulin in neurites of developing neurons (Figure 2A−C, Figure 3) are consistent with the reported distribution of these cytoskeleton proteins obtained by immunofluorescence microscopy with antibodies,[39,40] or live-cell FLM using SiR-actin and SiR-tubulin dyes.[26] In developing neurons, tubulin is present in the cell body and all along the entire length of the neurites, whereas F-actin is concentrated in the outgrowths of new neurites at the periphery of the cell body, in some specific regions along the neurites and in the growth cones (Figure 2A−C, Figure 3).

As expected from its ubiquitous intracellular distribution, potassium images depict the entire cellular structure. Interestingly, the high spatial resolution of the SXRF images reveals that the nuclear envelope is particularly rich in K (Figure 2D), as observed in previous experiments.[15] Although the explanation for this observation is not clear, it may be due to the presence of potassium channels in the nuclear envelope. Some neuronal structures are mainly revealed by the potassium distribution but not by the protein-labeling. Axonal varicosities, which are enlarged bulbs along the length of the axon, are also called axonal *en passant boutons*, are revealed thanks to the K image (Figures 2D green arrows).[47,48]

We observed higher Zn levels in the nucleus than in the cytoplasm (Figure 2D). Zn higher concentration in the nucleus compared to the cytoplasm have been consistently observed,[33,46,49] and may be primarily due to zinc critical role in nuclear functions (e.g., transcription factors such as zinc-finger proteins, DNA and RNA polymerases, DNA repair enzymes, ...).

The cytoplasm and the nuclear regions of neurons are relatively thick, and organelles and nuclear structures may be superimposed. For correlative purposes in thick cell regions, 3D imaging is required to distinguish the different structures within the neuronal volume. However, in thinner regions such as axons and dendrites the 2D correlative imaging is more straightforward.

The site of contact between the neurites from two neurons shows a presynaptic axonal varicosity and its postsynaptic counterpart (Figure 3A, top panel). The postsynaptic protrusion contains high levels of F-actin with a broad distribution and tubulin with a narrower distribution, whereas the axonal varicosity contains some F-actin and tubulin, but only along the neurite (Figures 3A and 3B). Zinc is present in the postsynaptic protrusion (Figure 3C), a result comparable to our previous work on freeze-dried samples showing high levels of Zn in the postsynapses.[25,28] Figure 3C also shows the presence of Zn in the axonal varicosity. Interestingly Cu is found only at the periphery of the F-actin distribution (Figure 3D). Copper and F-actin colocalization has also been previously observed in postsynaptic compartments,[25] although here the local distribution is better defined with Cu-enriched regions at the edges of the dendritic protrusion and the axonal varicosities (Figure 3D, top and bottom panels). The K and Cu overlay images further confirm the edge distribution that Cu is localized in limited regions within or at the edge of the K structures (Figure 3E).

In growth cones (Figure 4), three regions can be distinguished according to the distribution of cytoskeleton proteins: the base of the growth cone, rich in tubulin; the center of the growth cone, rich in F-actin; the top of the growth cone, without tubulin or F-actin signal but clearly observed by the K distribution (Figures 4A and 4E). At the bottom of the growth cone, the tubulin-rich region shows the presence of P, S, K, and Zn. Ca and Fe are present in round vesicle-like structures at the center of the growth cone. Ca and Fe round structures are similar in size, in micrometer range, but are not colocalized (Figure 4F). The upper region of the growth cone does not contain such Ca and Fe vesicles. The zinc distribution marks the boundary between the F-actin rich region and the top of the growth cone (Figure 4D). Zinc colocalizes with S (Figure 4E).

These data indicate a compartmentalization of the elements at the scale of the growth cones and suggest that each element may have specific functions in the neuronal development, either in structural dynamics, energy metabolism, or cell signaling. For example, P, S, K, and Zn are constituents of the entire neuronal growth cone structure. Meanwhile, Ca and Fe images show that these elements are confined in micron-sized circular structures, suggesting that these elements are probably required for cell functions in specific organelles such as mitochondria or lysosomes.

Although cryogenic sample preparation results in a better preservation of the elemental distribution than chemical fixation, it may not be free of damage, especially at the nanoscale. For example, the distribution of the diffusible element K, as shown in Figure 4D, sometimes shows heterogeneous structures like nanostrings that are difficult to interpret from a biological perspective.

■ CONCLUSIONS AND PERSPECTIVES

We have developed a protocol for correlative metal/protein imaging in cultured cells using cryo-FLM for protein distribution and cryo-SXRF, for element localization. This methodological workflow is fully cryogenic, preserving the native distribution of chemical elements and avoiding any structural distortion. This cryo-correlative protocol has been validated by imaging developing neurons. The major problems of sample preparation or recording positions have been solved and the methodology can be applied to a wide panel of research studies in cell biology to deepen the knowledge of metal function in physiological or pathological conditions.

One of the limitations of the method is that cryo-FLM is performed with a spatial resolution in the micrometer range, while cryo-SXRF spatial resolution can be as good as a few tens of nanometers. This limitation is similar to that of cryo-CLEM using an epifluorescence cryo-microscope and electron microscopy. The next step for improvement could be to perform super resolution cryo-FLM, similar to recent CLEM developments.[50]

Another correlative imaging strategy that can be implemented is the use of SXRF to simultaneously image metals and proteins genetically tagged with a metal.[49,51] For example, lanthanide-binding tags have been used to label and image the localization of the outer membrane protein A or the cytosolic protein ubiquitin in *E. coli*.[51] The major advantage of this approach is that correlative imaging can be performed in a single step and the process of correlation is straightforward. The main limitation today is the design of the metal tags for specific proteins, but efforts in this promising field should be followed.

In this article we have described the methodology for accurate protein/metal correlative cryo-imaging in 2D. Other very interesting approaches have been developed to investigate the intracellular distribution of the elements in 3D. For example, cryogenic 3D imaging combining SXRF and synchrotron X-ray holography has allowed the quantification of the elemental content in different organelles in frozen hydrated macrophages, close to their native state.[20] Another study correlates cryo-epifluorescence microscopy, 3D cryo-soft X-ray tomography and 3D hard X-ray cryo-fluorescence to elucidate the fate of an iridium-based anticancer compound, showing that it targets the mitochondria.[16] This work paves the way for future developments in 3D correlative imaging based on cryo-SXRF tomography, which could be combined with super resolution cryo-FLM.

■ METHODS

Culture of Primary Rat Hippocampal Neurons

Primary rat hippocampal neurons from 18-day-old embryonic rats (E18, Sprague−Dawley) were dissociated and cultured on an astrocyte feeder layer, as adapted from the protocol described by Kaech and Banker.[28,52] Experimental procedures complied with the European Guide for the Care and Use of Laboratory Animals and the animal care guidelines issued by the University of Bordeaux's animal experimentation ethics committee.

Silicon nitride membranes, which are thin, flat, and rigid substrates compatible with SXRF analyses, have been used as cell culture substrates.[25,26,32] In this study, we used silicon nitride membranes consisting of a 1.5 mm square window with a thickness of 500 nm produced on 5 mm square silicon wafers with thickness of 200 μm (SiRN-5.0−200−1.5−500, Silson Ltd.). These membranes have been specially designed with an orientation mark consisting of a smaller square membrane (0.5 μm) in one of the corners of the silicon wafer. Sterile silicon nitride membranes were coated with 1 mg/mL poly-L-lysine (PLL) in 0.1 M borate buffered saline solution (both from Sigma-Aldrich, France), for 2h at 37 °C, washed twice with sterile ultratrace elemental analysis grade water (Fisher Scientific, France) and covered with neurobasal culture medium (Gibco, France), to avoid PLL drying and crystal formation. Membranes were stored at 37 °C in the incubator until use, the day after coating. Dissociated neurons were seeded at a homogeneous density of 20 000 neurons/cm^2 onto the silicon nitride membranes using neurobasal medium. One hour after seeding, the membranes were transferred to a Petri dish containing an astrocyte feeder layer and returned to the incubator. Neurons were cultured for 3 days in vitro (DIV3) at 37 °C, 5% CO$_2$, in neurobasal medium supplemented with 2 mM L-glutamine and neuronal supplement B27.

Fluorescent Labeling of Proteins

Neurons at DIV3 were labeled for F-actin and tubulin imaging using fluorescent probes developed for live-cell microscopy. For dual-color imaging, we combined the actin fluorescent dye LIVE590 (Aberrior, Germany) emitting at green wavelengths (λ absorption 585 nm; λ fluorescence 609 nm) with SiR-tubulin (Spirochrome, Switzerland) emitting at far-red wavelengths (λ absorption 652 nm; λ fluorescence 674 nm). LIVE590-actin uses the F-actin binding ligand jasplakinolide[53] while SiR-tubulin is based on the microtubule binding drug docetaxel.[44,45] Following the instructions provided by the manufacturers, neurons were exposed to 0.5 μM LIVE590-actin and 1 μM SiR-tubulin. Fluorescent probes were added directly to the culture medium, and samples were incubated at 37 °C and 5% CO$_2$ for 1 h. Labeling was carried out just prior to plunge freezing.

Cryo-Preservation

Samples were cryo-preserved by plunge-freezing and stored in liquid nitrogen until analysis.[25,26,32,54] Plunge freezing must be carried out rapidly to maintain cells in their native state, and follow the three steps below.

First, after live-cell labeling, samples are quickly rinsed by immersion in a warmed ammonium acetate buffer solution (Sigma-Aldrich, France). The ammonium acetate solution is prepared with ultratrace elemental analysis grade water and adjusted to the same pH and osmolarity as the neurobasal culture medium (pH 7.4 and 240 mOsm). This rinse is performed to remove the extracellular inorganic salts present in the culture medium using a purely organic solution, while maintaining the physiological pH and osmolarity. The extracellular neurobasal medium has a very high sodium chloride (3 g/L) and potassium chloride (0.4 g/L) content, which saturates the count rate of the XRF detector, preventing the detection of intracellular trace elements.

Second, it is necessary to blot the remaining rinse solution from the membrane surface. The aim of this is to obtain a thin layer of ice on

the sample surface. The ice layer must be as thin as possible to allow cryo-FLM and cryo-SXRF imaging. Thick extracellular ice layers would result in multiple background light scattering during cryo-FLM, masking the specific fluorescence of the tagged proteins. During cryo-SXRF, the thick ice layers absorb the X-ray fluorescence signal and increase the Compton scattering background, thus reducing the overall analytical sensitivity. For this step, we used the blotting capability of the automated vitrification system, the Vitrobot Marck IV apparatus from FEI (U.S.A.). This machine blots the membranes, front and back, by absorbing the liquid at the bottom of the silicon frame of the wafers and avoiding direct contact with the neurons. An ultra-absorbent ashless filter paper (Whatman, U.S.A.) was used and we blotted 1 time for 4 s and with force 1 setting on the Vitrobot system. The humidity of chamber was set at 100% for processing and the temperature to 25 °C.

The final step involves rapid immersion of the sample in liquid ethane, cooled by thermal contact with liquid nitrogen. The Vitrobot system ensure fast, controlled plunge-freezing. After cryo-fixation, the membranes are transferred to cryo-storage tubes (Nunc, Fisher Scientific, France), which are kept in liquid nitrogen until further analysis.

Cryo-Fluorescence Light Microscopy (cryo-FLM)

Membranes stored in liquid nitrogen are transferred to a custom wide-field EM CryoCLEM microscope (Leica Microsystems, Germany). This system contains a HC PL APO 50x/0,90 NA cryogenic objective (Leica Microsystems, Germany), and an Orca-Fusion BT camera (Hamamatsu Photonics, France). For transfer under cryogenic conditions, a sample holder adapted to silicon nitride membranes and a cryo-transfer chamber, both designed by Leica, were used to keep samples in liquid nitrogen throughout the process. The cryo-fluorescence microscope is equipped with an automated system controlling the chamber temperature, set at −190 °C, by injection of liquid nitrogen.

An important step in this workflow is to be able to find the neurons of interest, imaged by cryo-FLM, later at the synchrotron beamline. The cryo-FLM system is controlled by Metamorph software (Molecular Devices, U.S.A.), which enables rapid acquisition of mosaics using a ND-Scan module. To obtain the coordinates of the imaged neurons, the orientation mark positioned on one of the corners of the silicon wafer is used as a reference point (0,0) and the horizontal and vertical coordinates (x,y) of the regions of interest are recorded during cryo-FLM acquisitions, relative to this reference point.[25]

The physical length of images was set to 211.25 μm square, working at 2048 pixels, and the pixel size was set at 103 nm. An Y3 filter (565 nm excitation, bandwidth 610/675 nm) and an Y5 filter (660 nm excitation, bandwidth 700/775 nm) were used to detect LIVE590-actin and SiR-tubulin, respectively.

A mosaic acquisition of the entire membrane (1.5 × 1.5 mm^2) at each wavelength is performed to record the position of all the regions of interest in the membrane. The cryo-FLM images presented in this article show projection of the maximum intensity of the acquired z-stack. After cryo-FLM, the samples are returned to the cryo-tubes and stored in liquid nitrogen. In this way, we can select, a posteriori, the same regions of interest to be imaged by SXRF.

Cryo-Synchrotron X-ray Fluorescence (cryo-SXRF) Imaging

SXRF measurements were performed at the European Synchrotron (ESRF) on beamline ID16A.[55] A monochromatic of 17.1 keV X-ray photons beam was focused to a size of 40 nm, providing a flux of 2.2 × 10^{11} photons/s. The instrument operates under a vacuum of ~10^{-8} mbar and the sample is cooled by an unforced flow of mixed liquid/gaseous nitrogen to a temperature of ~108 K.

Samples were maintained under cryogenic conditions during transfer and acquisition. Samples were raster scanned in a continuous mode with an integration time of 100 ms/pixel and a step size of 50 nm/pixel. The XRF signal was recorded with two large solid angle detectors, based on multielement silicon drift diodes, placed at approximately 90° at either side of the incident beam. The summed X-ray fluorescence spectra from the multielement detectors were

fitted and calibrated against the signal derived from a thin film X-ray fluorescence standard (AXO Dresden GmbH, Germany) with Python scripts using the PyMCA library.[56] The resulting areal mass density distributions of the detected chemical elements were saved as 32-bits tiff images.

For correlative image overlay we used ICY software (http://icy.bioimageanalysis.org) and the eC-CLEM plugin.[57]

■ ASSOCIATED CONTENT

ⓢ Supporting Information

The Supporting Information is available free of charge at https://pubs.acs.org/doi/10.1021/cbmi.4c00038.

> Figure S1. Correlative imaging of proteins (tubulin and F-actin) and chemical elements in developing neurons. (A) Overlay images of F-actin (green) and tubulin (red) distributions by confocal microscopy in living conditions. (B) Overlay images of F-actin (green) and tubulin (red) distributions by STED microscopy in living conditions in the region framed in A. (C) Elemental distributions obtained by cryo-SXRF of the growth cone, pointed by the arrow in B. Figure S2. Correlative imaging of proteins (tubulin and F-actin) and chemical elements in developing neurons. (A) Overlay images of F-actin (green) and tubulin (red) distributions by confocal microscopy in living conditions. (B) Zoom of the overlay images of the region framed in A. (C) Elemental distributions obtained by cryo-SXRF of the protrusions pointed by the arrow in B. Figure S3. Correlative imaging of proteins (tubulin and F-actin) and chemical elements in developing neurons. (A) Overlay images of F-actin (green) and tubulin (red) distributions by confocal microscopy in living conditions. (B) Overlay images of F-actin (green) and tubulin (red) distributions by STED microscopy in living conditions in the region framed in A. (C) Elemental distributions obtained by cryo-SXRF of the growth cone, pointed by the arrow in B (PDF)

■ AUTHOR INFORMATION

Corresponding Author

Asuncion Carmona − *Université Bordeaux, CNRS, LP2IB, Chemical Imaging and Speciation, UMR 5797, 33170 Gradignan, France;* ⊙ orcid.org/0000-0002-9253-4581; Email: asuncion.carmona@u-bordeaux.fr

Authors

Richard Ortega − *Université Bordeaux, CNRS, LP2IB, Chemical Imaging and Speciation, UMR 5797, 33170 Gradignan, France;* ⊙ orcid.org/0000-0003-1692-5406

Mónica Fernández-Monreal − *Université Bordeaux, CNRS, INSERM, Bordeaux Imaging Center, BIC, 33000 Bordeaux, France*

Noémie Pied − *Université Bordeaux, CNRS, INSERM, Bordeaux Imaging Center, BIC, 33000 Bordeaux, France*

Stéphane Roudeau − *Université Bordeaux, CNRS, LP2IB, Chemical Imaging and Speciation, UMR 5797, 33170 Gradignan, France;* ⊙ orcid.org/0000-0002-4539-9380

Peter Cloetens − *ESRF, The European Synchrotron, 38042 Grenoble, France*

Complete contact information is available at:
https://pubs.acs.org/10.1021/cbmi.4c00038

■ REFERENCES

(1) Zoroddu, M. A.; Aaseth, J.; Crisponi, G.; Medici, S.; Peana, M.; Nurchi, V. M. The essential metals for humans: a brief overview. *J. Inorg. Biochem.* **2019**, *195*, 120−129.

(2) Jomova, K.; Makova, M.; Alomar, S. Y.; Alwasel, S. H.; Nepovimova, E.; Kuca, K.; Rhodes, C. J.; Valko, M. Essential metals in health and disease. *Chem. Biol. Interact.* **2022**, *367*, No. 110173.

(3) Andreini, C.; Bertini, I.; Cavallaro, G.; Holliday, G. L.; Thornton, J. M. Metal ions in biological catalysis: from enzyme databases to general principles. *J. Biol. Inorg. Chem.* **2008**, *13* (8), 1205−18.

(4) Lothian, A.; Hare, D. J.; Grimm, R.; Ryan, T. M.; Masters, C. L.; Roberts, B. R. Metalloproteomics: principles, challenges and applications to neurodegeneration. *Front Aging Neurosci.* **2013**, *5*, 35.

(5) Acevedo, K.; Masaldan, S.; Opazo, C. M.; Bush, A. I. Redox active metals in neurodegenerative diseases. *J. Biol. Inorg. Chem.* **2019**, *24* (8), 1141−1157.

(6) Frye, R. E.; Cakir, J.; Rose, S.; Delhey, L.; Bennuri, S. C.; Tippett, M.; Palmer, R. F.; Austin, C.; Curtin, P.; Arora, M. Early life metal exposure dysregulates cellular bioenergetics in children with regressive autism spectrum disorder. *Transl Psychiatry.* **2020**, *10* (1), 223.

(7) Doroszkiewicz, J.; Farhan, J. A.; Mroczko, J.; Winkel, I.; Perkowski, M.; Mroczko, B. Common and Trace Metals in Alzheimer's and Parkinson's Diseases. *Int. J. Mol. Sci.* **2023**, *24* (21), 15721.

(8) Zhang, Y. Y.; Li, X. S.; Ren, K. D.; Peng, J.; Luo, X. J. Restoration of metal homeostasis: a potential strategy against neurodegenerative diseases. *Ageing Res. Rev.* **2023**, *87*, No. 101931.

(9) Sisley, E. K.; Hale, O. J.; Styles, I. B.; Cooper, H. J. Native Ambient Mass Spectrometry Imaging of Ligand-Bound and Metal-Bound Proteins in Rat Brain. *J. Am. Chem. Soc.* **2022**, *144* (5), 2120−2128.

(10) Perry, W. J.; Weiss, A.; Van de Plas, R.; Spraggins, J. M.; Caprioli, R. M.; Skaar, E. P. Integrated molecular imaging technologies for investigation of metals in biological systems: A brief review. *Curr. Opin Chem. Biol.* **2020**, *55*, 127−135. Apr

(11) Roudeau, S.; Carmona, A.; Ortega, R. Multimodal and multiscale correlative elemental imaging: From whole tissues down to organelles. *Curr. Opin Chem. Biol.* **2023**, *76*, No. 102372.

(12) Pushie, M. J.; Sylvain, N. J.; Hou, H.; Hackett, M. J.; Kelly, M. E.; Webb, S. M. X-ray fluorescence microscopy methods for biological tissues. *Metallomics.* **2022**, *14* (6), No. mfac032.

(13) Kapishnikov, S.; Grolimund, D.; Schneider, G.; Pereiro, E.; McNally, J. G.; Als-Nielsen, J.; Leiserowitz, L. Unraveling heme detoxification in the malaria parasite by in situ correlative X-ray fluorescence microscopy and soft X-ray tomography. *Sci. Rep.* **2017**, *7* (1), 7610.

(14) De Samber, B.; Meul, E.; Laforce, B.; De Paepe, B.; Smet, J.; De Bruyne, M.; De Rycke, R.; Bohic, S.; Cloetens, P.; Van Coster, R.; Vandenabeele, P.; Vanden Berghe, T. Nanoscopic X-ray fluorescence imaging and quantification of intracellular key-elements in cryofrozen Friedreich's ataxia fibroblasts. *PLoS One.* **2018**, *13* (1), No. e0190495.

(15) Carmona, A.; Zogzas, C. E.; Roudeau, S.; Porcaro, F.; Garrevoet, J.; Spiers, K. M.; Salomé, M.; Cloetens, P.; Mukhopadhyay, S.; Ortega, R. SLC30A10 Mutation Involved in Parkinsonism Results in Manganese Accumulation within Nano-vesicles of the Golgi Apparatus. *ACS Chem. Neurosci.* **2019**, *10* (1), 599−609.

(16) Conesa, J. J.; Carrasco, A. C.; Rodríguez-Fanjul, V.; Yang, Y.; Carrascosa, J. L.; Cloetens, P.; Pereiro, E.; Pizarro, A. M. Unambiguous Intracellular Localization and Quantification of a Potent Iridium Anticancer Compound by Correlative 3D Cryo X-Ray Imaging. *Angew. Chem., Int. Ed. Engl.* **2020**, *59* (3), 1270−1278.

(17) Rumancev, C.; Gräfenstein, A.; Vöpel, T.; Stuhr, S.; von Gundlach, A. R.; Senkbeil, T.; Garrevoet, J.; Jolmes, L.; König, B.; Falkenberg, G.; Ebbinghaus, S.; Schroeder, W. H.; Rosenhahn, A. X-ray fluorescence analysis of metal distributions in cryogenic biological samples using large-acceptance-angle SDD detection and continuous scanning at the Hard X-ray Micro/Nano-Probe beamline P06 at PETRA III. *J. Synchrotron Radiat.* **2020**, *27* (1), 60−66.

(18) Roudeau, S.; Carmona, A.; Perrin, L.; Ortega, R. Correlative organelle fluorescence microscopy and synchrotron X-ray chemical element imaging in single cells. *Anal Bioanal Chem.* **2014**, *406* (27), 6979−91.

(19) Yang, Y.; Fus, F.; Pacureanu, A.; da Silva, J. C.; De Nolf, W.; Biot, C.; Bohic, S.; Cloetens, P. Three-Dimensional Correlative Imaging of a Malaria-Infected Cell with a Hard X-ray Nanoprobe. *Anal. Chem.* **2019**, *91* (10), 6549−6554.

(20) Gramaccioni, C.; Yang, Y.; Pacureanu, A.; Vigano, N.; Procopio, A.; Valenti, P.; Rosa, L.; Berlutti, F.; Bohic, S.; Cloetens, P. Cryo-nanoimaging of Single Human Macrophage Cells: 3D Structural and Chemical Quantification. *Anal. Chem.* **2020**, *92* (7), 4814−4819.

(21) Gustavsson, N.; Paulus, A.; Martinsson, I.; Engdahl, A.; Medjoubi, K.; Klementiev, K.; Somogyi, A.; Deierborg, T.; Borondics, F.; Gouras, G. K.; Klementieva, O. Correlative optical photothermal infrared and X-ray fluorescence for chemical imaging of trace elements and relevant molecular structures directly in neurons. *Light Sci. Appl.* **2021**, *10* (1), 151.

(22) Tardillo Suárez, V.; Gallet, B.; Chevallet, M.; Jouneau, P. H.; Tucoulou, R.; Veronesi, G.; Deniaud, A. Correlative transmission electron microscopy and high-resolution hard X-ray fluorescence microscopy of cell sections to measure trace element concentrations at the organelle level. *J. Struct Biol.* **2021**, *213* (3), No. 107766.

(23) Lemelle, L.; Simionovici, A.; Colin, P.; Knott, G.; Bohic, S.; Cloetens, P.; Schneider, B. L. Nano-imaging trace elements at organelle levels in substantia nigra overexpressing α-synuclein to model Parkinson's disease. *Commun. Biol.* **2020**, *3* (1), 364.

(24) Nagarajan, S.; Poyer, F.; Fourmois, L.; Naud-Martin, D.; Medjoubi, K.; Somogyi, A.; Schanne, G.; Henry, L.; Delsuc, N.; Policar, C.; Bertrand, H. C.; Mahuteau-Betzer, F. Cellular Detection of a Mitochondria Targeted Brominated Vinyl Triphenylamine Optical Probe (TP-Br) by X-Ray Fluorescence Microscopy. *Chem. Eur. J.* **2022**, *28* (15), No. e202104424.

(25) Domart, F.; Cloetens, P.; Roudeau, S.; Carmona, A.; Verdier, E.; Choquet, D.; Ortega, R. Correlating STED and synchrotron XRF nano-imaging unveils cosegregation of metals and cytoskeleton proteins in dendrites. *Elife.* **2020**, *9*, No. e62334.

(26) Carmona, A.; Chen, S.; Domart, F.; Choquet, D.; Ortega, R. Imaging the structural organization of chemical elements in growth cones of developing hippocampal neurons. *Metallomics.* **2022**, *14* (1), No. mfab073.

(27) Gräfenstein, A.; Rumancev, C.; Pollak, R.; Hämisch, B.; Galbierz, V.; Schroeder, W. H.; Garrevoet, J.; Falkenberg, G.; Vöpel, T.; Huber, K.; Ebbinghaus, S.; Rosenhahn, A. Spatial Distribution of Intracellular Ion Concentrations in Aggregate-Forming HeLa Cells Analyzed by μ-XRF Imaging. *ChemistryOpen.* **2022**, *11* (4), No. e202200024.

(28) Ortega, R.; Roudeau, S.; Carmona, A. Correlative nano-imaging of metals and proteins in primary neurons by synchrotron X-ray fluorescence and STED super resolution microscopy: Experimental validation. *J. Neurosci Methods.* **2022**, *381*, No. 109702.

(29) Chwiej, J.; Szczerbowska-Boruchowska, M.; Lankosz, M.; Wojcik, S.; Falkenberg, G.; Stegowski, Z.; Setkowicz, Z. Preparation of tissue samples for X-ray fluorescence microscopy. *Spectrochimica Acta Part B: Atomic Spectroscopy* **2005**, *60* (12), 1531−1537.

(30) Hackett, M. J.; McQuillan, J. A.; El-Assaad, F.; Aitken, J. B.; Levina, A.; Cohen, D. D.; Siegele, R.; Carter, E. A.; Grau, G. E.; Hunt, N. H.; Lay, P. A. Chemical alterations to murine brain tissue induced by formalin fixation: implications for biospectroscopic imaging and mapping studies of disease pathogenesis. *Analyst.* **2011**, *136* (14), 2941−52.

(31) De Samber, B.; Vanblaere, S.; Evens, R.; et al. Dual detection X-ray fluorescence cryotomography and mapping on the model organism Daphnia magna. *Powder Diffraction.* **2010**, *25* (2), 169−174.

(32) Perrin, L.; Carmona, A.; Roudeau, S.; Ortega, R. Evaluation of sample preparation methods for single cell quantitative elemental imaging using proton or synchrotron radiation focused beams. *Journal of Analytical Atomic Spectrometry.* **2015**, *30*, 2525−2532.

(33) Jin, Q.; Paunesku, T.; Lai, B.; Gleber, S. C.; Chen, S. I.; Finney, L.; Vine, D.; Vogt, S.; Woloschak, G.; Jacobsen, C. Preserving elemental content in adherent mammalian cells for analysis by synchrotron-based x-ray fluorescence microscopy. *J. Microsc.* **2017**, *265* (1), 81−93.

(34) Carmona, A.; Porcaro, F.; Somogyi, A.; Roudeau, S.; Domart, F.; Medjoubi, K.; Aubert, M.; Isnard, H.; Nonell, A.; Rincel, A.; Paredes, E.; Vidaud, C.; Malard, V.; Bresson, C.; Ortega, R. Cytoplasmic aggregation of uranium in human dopaminergic cells after continuous exposure to soluble uranyl at non-cytotoxic concentrations. *Neurotoxicology.* **2021**, *82*, 35−44.

(35) Chen, S.; Deng, J.; Yuan, Y.; Flachenecker, C.; Mak, R.; Hornberger, B.; Jin, Q.; Shu, D.; Lai, B.; Maser, J.; Roehrig, C.; Paunesku, T.; Gleber, S. C.; Vine, D. J.; Finney, L.; VonOsinski, J.; Bolbat, M.; Spink, I.; Chen, Z.; Steele, J.; Trapp, D.; Irwin, J.; Feser, M.; Snyder, E.; Brister, K.; Jacobsen, C.; Woloschak, G.; Vogt, S. The Bionanoprobe: hard X-ray fluorescence nanoprobe with cryogenic capabilities. *J. Synchrotron Radiat.* **2014**, *21* (1), 66−75.

(36) Cotte, M.; Pouyet, E.; Salomé, M.; Rivard, C.; De Nolf, W.; Castillo-Michel, H.; Fabris, T.; Monico, L.; Janssens, K.; Wang, T.; Sciau, P.; Verger, L.; Cormier, L.; Dargaud, O.; Brun, E.; Bugnazet, D.; Fayard, B.; Hesse, B.; Pradas del Real, A. E.; Veronesi, G.; Langlois, J.; Balcar, N.; Vandenberghe, Y.; Solé, V. A.; Kieffer, J.; Barrett, R.; Cohen, C.; Cornu, C.; Baker, R.; Gagliardini, E.; Papillon, E.; Susini, J. The ID21 X-Ray and Infrared Microscopy Beamline at the ESRF: Status and Recent Applications to Artistic Materials. *J. Anal. At. Spectrom.* **2017**, *32*, 477−493.

(37) Steinmann, R. G.; Martinez-Criado, G.; Salomon, D.; Vitoux, H.; Tucoulou, R.; Villanova, J.; Laboure, S.; Eymery, J.; Segura-Ruiz, J. A helium mini-cryostat for the nanoprobe beamline ID16B at ESRF: characteristics and performance. *J. Synchrotron Radiat.* **2020**, *27* (4), 1074−1079.

(38) Jun, S.; Ro, H. J.; Bharda, A.; Kim, S. I.; Jeoung, D.; Jung, H. S. Advances in Cryo-Correlative Light and Electron Microscopy:

(39) Kapitein, L. C.; Hoogenraad, C. C. Building the Neuronal Microtubule Cytoskeleton. *Neuron.* **2015**, *87* (3), 492−506.

(40) Leterrier, C. A Pictorial History of the Neuronal Cytoskeleton. *J. Neurosci.* **2021**, *41* (1), 11−27.

(41) Tojima, T.; Hines, J. H.; Henley, J. R.; Kamiguchi, H. Second messengers and membrane trafficking direct and organize growth cone steering. *Nat. Rev. Neurosci.* **2011**, *12* (4), 191−203.

(42) Li, Y.; Almassalha, L. M.; Chandler, J. E.; Zhou, X.; Stypula-Cyrus, Y. E.; Hujsak, K. A.; Roth, E. W.; Bleher, R.; Subramanian, H.; Szleifer, I.; Dravid, V. P.; Backman, V. The effects of chemical fixation on the cellular nanostructure. *Exp. Cell Res.* **2017**, *358* (2), 253−259.

(43) Tamada, H.; Blanc, J.; Korogod, N.; Petersen, C. C.; Knott, G. W. Ultrastructural comparison of dendritic spine morphology preserved with cryo and chemical fixation. *Elife.* **2020**, *9*, No. e56384.

(44) Lukinavičius, G.; Reymond, L.; D'Este, E.; Masharina, A.; Göttfert, F.; Ta, H.; Güther, A.; Fournier, M.; Rizzo, S.; Waldmann, H.; Blaukopf, C.; Sommer, C.; Gerlich, D. W.; Arndt, H. D.; Hell, S. W.; Johnsson, K. Fluorogenic probes for live-cell imaging of the cytoskeleton. *Nat. Methods.* **2014**, *11* (7), 731−3.

(45) Lukinavičius, G.; Reymond, L.; Umezawa, K.; Sallin, O.; D'Este, E.; Göttfert, F.; Ta, H.; Hell, S. W.; Urano, Y.; Johnsson, K. Fluorogenic Probes for Multicolor Imaging in Living Cells. *J. Am. Chem. Soc.* **2016**, *138* (30), 9365−8.

(46) Bissardon, C.; Proux, O.; Gazze, S. A.; Filhol, O.; Toubhans, B.; Sauzéat, L.; Bouchet, S.; Lewis, A. R.; Maffeis, T.; Hazemann, J. L.; Bayat, S.; Cloetens, P.; Conlan, R. S.; Charlet, L.; Bohic, S. Intracellular Fate of Sub-Toxic Concentration of Functionalized Selenium Nanoparticles in Aggressive Prostate Cancer Cells. *Nanomaterials (Basel).* **2023**, *13* (23), 2999.

(47) Giachello, C. N.; Montarolo, P. G.; Ghirardi, M. Synaptic functions of invertebrate varicosities: what molecular mechanisms lie beneath. *Neural Plast.* **2012**, *2012*, 1−14.

(48) Gu, C. Rapid and Reversible Development of Axonal Varicosities: A New Form of Neural Plasticity. *Front Mol. Neurosci.* **2021**, *14*, No. 610857.

(49) Victor-Lovelace, T. W.; Miller, L. M. The development and use of metal-based probes for X-ray fluorescence microscopy. The development and use of metal-based probes for X-ray fluorescence microscopy. *Metallomics.* **2022**, *14* (12), No. mfac093.

(50) van den Dries, K.; Fransen, J.; Cambi, A. Fluorescence CLEM in biology: historic developments and current super-resolution applications. *FEBS Lett.* **2022**, *596* (19), 2486−2496.

(51) Victor, T. W.; O'Toole, K. H.; Easthon, L. M.; Ge, M.; Smith, R. J.; Huang, X.; Yan, H.; Chu, Y. S.; Chen, S.; Gursoy, D.; Ralle, M.; Imperiali, B.; Allen, K. N.; Miller, L. M. Lanthanide-Binding Tags for 3D X-ray Imaging of Proteins in Cells at Nanoscale Resolution. Lanthanide-Binding Tags for 3D X-ray Imaging of Proteins in Cells at Nanoscale Resolution. *J. Am. Chem. Soc.* **2020**, *142* (5), 2145−2149.

(52) Kaech, S.; Banker, G. Culturing hippocampal neurons. *Nat. Protoc.* **2006**, *1* (5), 2406−15.

(53) Belov, V. N.; Stoldt, S.; Rüttger, F.; John, M.; Seikowski, J.; Schimpfhauser, J.; Hell, S. W. Synthesis of Fluorescent Jasplakinolide Analogues for Live-Cell STED Microscopy of Actin. *J. Org. Chem.* **2020**, *85* (11), 7267−7275.

(54) Perrin, L.; Roudeau, S.; Carmona, A.; Domart, F.; Petersen, J. D.; Bohic, S.; Yang, Y.; Cloetens, P.; Ortega, R. Zinc and Copper Effects on Stability of Tubulin and Actin Networks in Dendrites and Spines of Hippocampal Neurons. *ACS Chem. Neurosci.* **2017**, *8* (7), 1490−1499.

(55) da Silva, J. C.; Pacureanu, A.; Yang, Y.; Bohic, S.; Morawe, C.; Barrett, R.; Cloetens, P. Efficient concentration of high-energy x-rays for diffraction-limited imaging resolution. *Optica* **2017**, *4*, 492−495.

(56) Sole, V. A.; Papillon, E.; Cotte, M.; Walter, P.; Susini, J. A multiplatform code for the analysis of energy-dispersive X-ray fluorescence spectra. *Spectrochimica Acta Part B: Atomic Spectroscopy* **2007**, *62*, 63−68.

(57) Paul-Gilloteaux, P.; Heiligenstein, X.; Belle, M.; Domart, M. C.; Larijani, B.; Collinson, L.; Raposo, G.; Salamero, J. eC-CLEM: flexible multidimensional registration software for correlative microscopies. *Nat. Methods.* **2017**, *14* (2), 102−103.